Nuclear Materials and Energy 47 (2026) 102128

Contents lists available at ScienceDirect

Nuclear Materials and Energy

journal homepage: www.elsevier.com/locate/nme

Fission products Sr and Ba in actinide (U, Th) chloride systems: Thermodynamic modelling, experimental investigation and application calculations

Dennis C. Alders *, Max J.A. IJszenga, Nick T.H. ter Veer, Elisa Capelli, Rudy J.M. Konings, Anna L. Smith

Reactor Physics and Nuclear Materials, Radiation Science & Technology Department, Faculty of Applied Sciences, Delft University of Technology, Mekelweg 15, Delft, 2629JB, The Netherlands

ARTICLE INFO

Keywords:
Molten salts
CALPHAD
Chlorides
Cerium
Uranium
Solid solution
Thorium
Simulant
Barium
Strontium

ABSTRACT

In this study, new insights into the solid state chemistry and melting behaviour of the $BaCl_2$—UCl_3 system are presented, building on results in the simulant system $BaCl_2$—$CeCl_3$. Our studies have revealed the solubility of U in the high-temperature β-phase of $BaCl_2$ (*i.e* $Ba_{1-x}U_xCl_{2+x}$) and an intermediate compound, $Ba_3U_2Cl_{12}$, which has led us to revisit or present for the first time the phase diagrams of this system accordingly. Furthermore, we present revised thermodynamic models for the systems $SrCl_2$—UCl_3, $AECl_2$—$ThCl_4$, UCl_3—$ThCl_4$ and NaCl—$ThCl_4$—UCl_3 (AE = Sr, Ba) based on existing literature data. With the constructed multi-component database NaCl—$ThCl_4$—UCl_3—$NdCl_3$—$CeCl_3$—$BaCl_2$—$SrCl_2$, the effect of fission products on the melting behaviour of molten chloride salts containing uranium and thorium is investigated through higher order phase equilibria calculations.

1. Introduction

The Molten Salt Reactor (MSR) is a type of nuclear reactor that, as the name implies, uses liquid salts as fuel and/or coolant. Characteristics that make molten salts an interesting option as nuclear fuel include a low vapour pressure and high thermal stability under operating conditions, operation at atmospheric pressure, a negative power feedback coefficient, high actinide solubility and potential for fission product retention [1,2]. All of these properties contribute to an increased inherent safety. Before large-scale adoption of MSR technology can be realized, some key knowledge gaps related to the complex chemistry of the molten fuel salt during operation with increasing burnup of the fissile material need to be addressed for a thorough safety assessment.

This work focuses more specifically on modelling the thermochemical behaviour of fission products barium and strontium in molten chloride fuels with actinide chlorides UCl_3 and $ThCl_4$, to assess their effect on the melting temperature of the salt.

Additionally, this work serves to illustrate the relevance of studies on simulant systems for the investigation of molten salt fuel systems. Targeted experiments (X-ray Diffraction (XRD) and Differential Scanning Calorimetry (DSC)), based on the known thermochemistry of the $BaCl_2$—$CeCl_3$ system, are carried out to elucidate the thermochemical behaviour of the $BaCl_2$—UCl_3 system and demonstrate the strength of using a simulant approach. Furthermore, thermodynamic models based on existing data in the literature are presented for the systems $SrCl_2$—UCl_3, $AECl_2$—$ThCl_4$ (AE = Sr, Ba), UCl_3—$ThCl_4$ and NaCl—$ThCl_4$—UCl_3. Finally, the thermodynamic model of the NaCl—$ThCl_4$—UCl_3—$NdCl_3$—$CeCl_3$—$SrCl_2$—$BaCl_2$ system constructed in this work is used to assess the behaviour of some fission products in actinide chloride systems.

2. Methods

2.1. Experimental techniques

2.1.1. Sample preparation

For the experiments carried out in this work, $BaCl_2$ was used as delivered by the supplier (Table 1), a small amount of UCl_3 was synthesized through the reduction reaction of UCl_4 with elemental silicon (Si) from an in-house prepared stock following the methodology presented by Rudel et al. [3]. This methodology relies on the formation of the

* Corresponding author.
E-mail addresses: d.c.alders@tudelft.nl (D.C. Alders), a.l.smith@tudelft.nl (A.L. Smith).

https://doi.org/10.1016/j.nme.2026.102128
Received 23 January 2026; Received in revised form 13 April 2026; Accepted 18 April 2026
Available online 27 April 2026

Table 1
Pure compounds used in the experiments in this work.

Compound	Supplier	CAS No	Reported purity	Melting point (DSC, K)	Melting point (lit., K)
$BaCl_2$	Merck	10361-37-2	99.999%	1235	1235 ± 2 [4]
UCl_3	In-house	10025-93-1	–	1112	1115 ± 2 [5]

volatile $SiCl_4$ upon reduction of UCl_4, allowing for easy separation based on boiling temperatures, and the synthesis was carried out in an evacuated borosilicate ampoule. The purity was verified by X-ray diffraction (XRD) and Differential Scanning Calorimetry (DSC), as shown in Table 1. No secondary impurity phases were detected, and the measured melting temperatures were found in excellent agreement with the data in the literature. Due to the sensitivity of the salts towards oxygen and water, all sample preparation was carried out inside a glove box under dry argon atmosphere (H_2O, O_2 < 5 ppm).

Weighing was carried out using a Mettler-Toledo XPE105DR balance with a 0.01 mg uncertainty. Sample preparation was conducted by mixing $BaCl_2$ and UCl_3 in the appropriate stoichiometric ratio in an agate mortar inside the dry argon atmosphere in the glovebox.

2.1.2. X-ray diffraction (XRD)

XRD measurements were carried out using a PANalytical X'pert pro diffractometer with a Cu-anode (0.4 mm × 12 mm line focus, 45 kV, 40 mA). Scattered X-ray intensities were measured with a real-time multi-step detector (X'Celerator). The angle 2θ was set to cover a range from 10 ° to 120 °. Measurements were typically performed for 7–8 h, with a step size of 0.0036 ° /s. Refinement of the measured XRD data was performed by applying the method of Rietveld, Loopstra and van Laar [6,7], using the FullProf software, Version 5.10 [8].

2.1.3. Differential scanning calorimetry (DSC)

The invariant temperatures in the investigated systems were measured using a Setaram multi-detector high-temperature calorimeter (MHTC-96 type) equipped with a 3D heat flux DSC module, capable of measuring up to 1673 K. Sample preparation was done by mixing end-members in the desired stoichiometric ratio. The sample containers consist of a nickel liner inside an gastight stainless steel crucible [9]. Equilibration of the sample was done in the calorimeter itself during the first heating cycle by heating the mixtures to a temperature above the melting points of both end members. Invariant equilibria were collected on the subsequent cycles.

The temperature was monitored throughout the experiments by a series of interconnected S-type thermocouples. The temperature on the heating ramp (10 K min^{-1}) was calibrated and corrected for the effect of the heating rate by measuring the melting points of standard high purity metals (In, Sn, Pb, Al, Ag, Au) at 2-4-6-8-10-12 K min^{-1}. The calibration procedure was performed as recommended by Höne et al. [10] and Gatta et al. [11]. The transition temperatures in the investigated phase diagrams were derived on the heating ramp as the onset temperature using tangential analysis of the recorded heat flow. The liquidus temperature of mixtures was derived from the peak extremum of the last thermal event. The uncertainty on the measured temperatures is estimated to be ± 5 K for pure compounds and ±10 K for mixtures.

2.2. Thermodynamic modelling

The thermodynamic modelling assessment of the molten salt systems was performed with the CALPHAD method [12] using the FactSage software, Version 8.2 [13]. Both literature and experimental data obtained in this work were used to optimize the excess parameters of the Gibbs energy functions of the phases present in the systems.

2.2.1. Stoichiometric compounds

The Gibbs energy function for stoichiometric compounds is dependent on the standard enthalpy of formation ($\Delta_f H^o_m(298)$), the standard entropy ($S^o_m(298)$) at the reference temperature of 298.15 K and the heat capacity ($C^o_{p,m}(T)$) as shown in Eq. (1) (with T in K).

$$G(T) = \Delta_f H^o_m(298) - S^o_m(298)T + \int_{298}^{T} C_{p,m}(T)dT - T\int_{298}^{T}\frac{C_{p,m}(T)}{T}dT \quad (1)$$

The isobaric heat capacity $C_{p,m}$ is expressed as a polynomial that takes the form of Eq. (2).

$$C_{p,m}(T) = a + bT + cT^{-2} + dT^2 \quad (2)$$

The thermodynamic data for all compounds are listed in Table 2, and the thermodynamic functions of $SrCl_2$, $BaCl_2$, $CeCl_3$ and UCl_3 were chosen to be consistent with previous works [14–20] and the JRC Molten Salt Database [21]. The thermodynamic functions used in this work for $ThCl_4$ were taken from the recommendations by Rand et al. [22], Capelli et al. [5] and ter Veer et al. [23].

2.2.2. Liquid solution

The excess Gibbs energy terms of the liquid solution are modelled using the quasi-chemical formalism in the quadruplet approximation as proposed by Pelton et al. [28] which has proven to be well-adapted to molten chloride and fluoride systems. This description assumes the existence of cation–anion quadruplets in the liquid, *i.e.* in the form of A-X-B-Y (A,B = cations; X,Y = anions), allowing for the modelling of short-range ordering. This formalism allows for the selection of the composition of maximum short-range ordering through its coordination numbers, corresponding to the minimum of the Gibbs energy that is often found near the composition of the lowest eutectic. By fixing either the cation–cation or anion–anion coordination number, the opposite coordination number is also obtained through Eq. (3), where q_i are the charges of the respective ions. In this work, we can simplify the description to the A-X-B-X quadruplet as chlorine is the only anion we consider. The coordination numbers used in the thermodynamic model presented in this work are given in Table 3.

$$\frac{q_A}{Z^A_{AB/XX}} + \frac{q_B}{Z^B_{AB/XX}} = 2\frac{q_X}{Z^X_{AB/XX}} \quad (3)$$

The excess parameters that are optimized are those related to the second-nearest neighbour exchange reactions as given in Eq. (4). The associated change in Gibbs energy of Eq. (4) is expressed in Eq. (5).

$$(A_2X_2)_{quad} + (B_2X_2)_{quad} \longrightarrow 2(ABX_2)_{quad} \qquad \Delta g_{AB/XX} \quad (4)$$

$$\Delta g_{AB/XX} = \Delta g^0_{AB/XX} + \Sigma_{i\geq 1} g^{i0}_{AB/XX}\chi^i_{AB/XX} + \Sigma_{j\geq 1} g^{0j}_{AB/XX}\chi^j_{BA/XX} \quad (5)$$

In Eq. (5) the terms $\Delta g^0_{AB/XX}$, $g^{i0}_{AB/XX}$ and $g^{0j}_{AB/XX}$ are composition-independent coefficients that may depend on temperature. The composition dependence of the Gibbs energy is apparent through $\chi_{AB/XX}$ as these are defined as per Eq. (6). In this equation X_{AA} is the cation–cation pair fraction, or the molar fraction of the quadruplet containing two cations A. For this binary system, $\{X_{AA} + X_{AB} + X_{BB}\}$ is equal to one.

$$\chi_{AB/XX} = \frac{X_{AA}}{X_{AA} + X_{AB} + X_{BB}} \quad (6)$$

The Gibbs energy functions used in this work to describe the liquid solutions are given in Table 4.

Table 2
Thermodynamic functions used in the CALPHAD model in this work. Optimized values are marked in bold.

Compound	$\Delta_f H^o_m(298)$ (J mol^{-1})	$S^o_m(298)$ (J K^{-1} mol^{-1})	$C_{p,m}(T)$ (J K^{-1} mol^{-1}) = a + bT + cT^{-2} + dT^2 a	b	c	d	e	Temperature range (K)	Source
UCl_3(s)	−863 700	163.9	106.967	−0.0208595	−129 994	$3.6389\cdot10^{-5}$		[298–1100]	[5]
UCl_3(l)	−846 616	152.919	151.1					[1100–2500]	[24]
$ThCl_4$(s)	−11863.0	183.499	120.293	0.0232672	−615 050			[298–1043]	[5,17]
$ThCl_4$(l)	−11620.4	176.93	184					[1043–2500]	[23]
$ThCl_4$(g)	−950 000	403.4	107.721	0.0002993	−573 880			[298–2000]	[23,25]
α-$BaCl_2$(s)	−855 200	123.7	69.371	$1.912548\cdot10^{-2}$	5882.698	$2.499235\cdot10^{-9}$		[298–1198]	[4]
β-$BaCl_2$(s)	−837 800	138.22	131					[1198–1234]	[4]
$BaCl_2$(l)	−821 950	151.07	109					[1234–2500]	[4]
$SrCl_2$(s)	−828850.4	114.809	79.4826	$-1.7920\cdot10^{-3}$	−440859.7	$1.798911\cdot10^{-5}$		[298–600]	[26]
			194.5439	−0.246728	−81598.6	$1.6616\cdot10^{-4}$		[600–1000]	[15]
			123.0096					[1000–1147]	[15]
$SrCl_2$(l)	−812 629	128.9515	104.6					[1147–2500]	[26]
$CeCl_3$(s)	−10597.0	151	90.9772	0.03581	−271 530			[298–1095]	[27]
$CeCl_3$(l)	−10061.0	200.17	161.05					[1095–3000]	[27]
$NdCl_3$(s)	−1,040,900	153.5	109.084	$1.6406\cdot10^{-2}$	−1,309,950			[298–1032]	[27]
$NdCl_3$(l)	−1,017,943.3	154.59	150					[1095–3000]	[27]
Intermediate compounds									
$Ba_3Ce_2Cl_{12}$	−47110.0	689.5	390.07	0.129	−525411.69	$7.4977\cdot10^{-9}$		[298–2500]	[14]
$Ba_3U_2Cl_{12}$(s)	−4 380 530	**650**	422.047	0.01565744	−242 340	$7.2785497705\cdot10^{-5}$		[298–1500]	This work
Ba_3ThCl_{10}(s)	−3 770 000	**555**	328.406	0.08064364	−597401.91	$7.49771\cdot10^{-9}$		[298–1500]	This work
$Ba_3Th_2Cl_{14}$(s)	−4 965 000	**738**	448.699	0.10391084	−12124.2	$7.49771\cdot10^{-9}$		[298–1500]	This work
$SrUCl_5$(s)	−1 686 819	**299**	186.444961	−0.022652036	−570 760	$5.44\cdot10^{-5}$		[298–1500]	This work

Table 3
Non-default coordination numbers used in the CALPHAD model presented in this work.

A	B	X	$Z^A_{AB/XX}$	$Z^B_{AB/XX}$	$Z^X_{AB/XX}$
Ba	U	Cl	6	3	1.5
Sr	U	Cl	6	3	1.5
Sr	Th	Cl	6	5	1.765
U	Th	Cl	6	4	1.333

Table 4
Excess Gibbs energy functions used in the CALPHAD model in this work for the liquid solution. Values have been optimized in this work.

AX	BX	$\Delta g^0_{AB/XX}$	$g^{10}_{AB/XX}$	$g^{01}_{AB/XX}$
$BaCl_2$	UCl_3	−8500 + 0.5T	3000 + T	2000−5T
$SrCl_2$	UCl_3	−4500−7T	500 + 11T	1000 + T
$BaCl_2$	$ThCl_4$	−10 000	−2000 + 0.5T	−10 000
$SrCl_2$	$ThCl_4$	−7800 + T	5500	−7000
UCl_3	$ThCl_4$	−4000		−6500

2.2.3. Solid solution modelling

The thermodynamic description of solid-solutions is done using the two-lattice polynomial model to be consistent with the description of the JRC Molten Salt Database (JRCMSD). The Gibbs Energy function of the solid-solutions are given in Table 5.

$$G(T) = X_A \cdot G^0_A + X_B \cdot G^0_B + X_A RT lnX_A + X_B RT lnX_B + \Delta G^{excess}_m \quad (7)$$

In Eq. (7), G^0_i are the end-member molar Gibbs energies, and X_i are the site molar fractions of the end-members A and B, respectively. The third and fourth terms in Eq. (7) represent the configurational entropy. The excess Gibbs energy, present in Eq. (7) as ΔG^{excess}_m, is defined as per Eq. (8).

$$\Delta G^{excess}_m = \Sigma_{i,j\geq1} X^i_A X^i_B L^{ij}_{AB} \quad (8)$$

The term L^{ij}_{AB} in Eq. (8) is an interaction coefficient that can be a function of temperature, if necessary. The terms X^i_A and X^j_B are the site molar fractions of end-members A and B. To model the homogeneity range of the $Na_{3x}Nd_{2-x}Cl_6$ phase, our previously published model was used [20]. The corresponding Gibbs energy functions are given in Table 5.

Table 5
Excess Gibbs energy functions used in the CALPHAD model in this work for the solid solution. Values have been optimized in this work.

A	B	L^{11}_{AB}	L^{21}_{AB}	L^{12}_{AB}
β-$BaCl_2$	UCl_3	−12 500 + 6T	−12 900 + 10T	21 000−10T
$SrCl_2$	UCl_3	15 000−15T		

Table 6
Higher order excess Gibbs energy parameters used in the thermodynamic database in this work.

System	Excess Gibbs Energy functions			Source
(Na,U,Th)Cl	$g^{001}_{ThNa(U)\|ClCl}$	=	−21 700	This work, [17]
	$g^{001}_{UTh(Na)\|ClCl}$	=	10 500	This work, [17]
	$g^{001}_{NaU(Th)\|ClCl}$	=	39 500	This work, [17]

2.3. Higher order solutions

The excess Gibbs energy parameters used for higher order systems are presented in Table 6. When the excess Gibbs energy parameters were not optimized in this work, but have been taken from the literature, the source of the excess parameters is given in the table. The pure end-member liquid salts investigated in this work can be classified in one of two categories: ionic liquids (NaCl) and liquids that form molecular complexes (such as UCl_3, $ThCl_4$). If the components in a system belong to the same group, that system is considered symmetrical (Kohler interpolation), otherwise it is asymmetrical (Toop interpolation) [29].

3. Results and discussion

3.1. The $BaCl_2$-UCl_3 system

The system $BaCl_2$−UCl_3 has been investigated experimentally by Desyatnik et al. [30] using Differential Thermal Analysis (DTA), and they identified an intermediate compound at composition x(UCl_3) = 0.33 with the stoichiometry Ba_2UCl_7. This is also the stoichiometry that was reported in the literature on the $BaCl_2$−$CeCl_3$ system by Storkonkin et al. [31], but as shown in our previous work [14] this is likely to correspond to the intermediate $Ba_3Ce_2Cl_{12}$ instead. Additionally, in the $BaCl_2$−$RECl_3$ (RE = Ce, Nd) systems, a high-temperature solid

Table 7
Comparison between cell parameters obtained for intermediates $Ba_3M_2Cl_{12}$ (M = Ce, Nd, U) (space group I4/m) in this work.

Source	Compound	a,b (Å)	c (Å)	V (Å^3)
This work	$Ba_3U_2Cl_{12}$	11.397(2)	21.797(4)	2831.2(6)
Alders et al. [15]	$Ba_3Nd_2Cl_{12}$	11.304(7)	21.635(3)	2764.5(25)
Alders et al. (XRD) [14]	$Ba_3Ce_2Cl_{12}$	11.363(1)	21.547(6)	2782.1(8)
Alders et al. (ND) [14]	$Ba_3Ce_2Cl_{12}$	11.336(9)	21.529(4)	2766.5(31)

solution with the composition $Ba_{1-x}RE_xCl_{2+x}$ (RE = Ce, Nd) is formed at low molar fractions of $RECl_3$ (≤ 0.25) [14,15]. Given the similarities between the chemistry of UCl_3 and $CeCl_3$ [20], we presume that such a solid solution also exists in the $BaCl_2-UCl_3$ system. To investigate this further, an experimental study was conducted with targeted experiments based on our knowledge of the $BaCl_2-RECl_3$ (RE = Ce, Nd) systems.

3.1.1. Experimental investigation

To investigate the existence of a solid solution at high temperature (with composition $Ba_{1-x}U_xCl_{2+x}$) a DSC measurement was performed at $x(UCl_3) = 0.2$, where we expect, by analogy with the $BaCl_2-UCl_3$ system, to see a thermal event of the solid solution $Ba_{1-x}U_xCl_{2+x}$ formation below the peritectic equilibrium measured by Desyatnik et al. [30]. The measured equilibria at this composition are shown on the phase diagram in Fig. 2. This measurement confirms the formation of the solid solution at elevated temperature through the measured equilibrium at $T = 920 \pm 10$ K. Moreover, the measured liquidus is in good agreement with the work of Desyatnik et al. [32]. Additionally, on the first cycle of the measurement, a small peak was detected at $T = 1060$ K, where Desyatnik et al. also measure an equilibrium. This peak disappeared on subsequent cycles, however, leading to its exclusion from the measured data.

Furthermore, an XRD measurement was performed on the same sample post-DSC to investigate the existence of the intermediate $Ba_3U_2Cl_{12}$. The profile refinement of the data is presented in Fig. 1. This refinement shows the presence of the low-temperature phase α-$BaCl_2$ (SGR *Pnma*), as well as the intermediate compound $Ba_3U_2Cl_{12}$. No crystal structure has been reported for the latter compound, so the structure of the analogous compounds $Ba_3Ce_2Cl_{12}$ and $Ba_3Nd_2Cl_{12}$, suggested in previous works [14,15] was used. A good agreement between the measured data and the calculated refinement is obtained, corroborating that the intermediate compound $Ba_3U_2Cl_{12}$ exists in this binary system. This contrasts with the interpretation of Desyatnik et al. [30] that the intermediate should be Ba_2UCl_7, but since their assessment did not include information on phase composition to support this, we believe that the thermal event they measure at $x(UCl_3) = 0.35$, $T = 980$ K is due to a kinetic effect that arises from cooling. The cell parameters of $Ba_3U_2Cl_{12}$ obtained from the refinement are presented in Table 7 and compared to the measured values for $Ba_3Ce_2Cl_{12}$ and $Ba_3Nd_2Cl_{12}$ (Chapter 4). The increase in cell volume of the intermediate compounds $Ba_3Nd_2Cl_{12}$, $Ba_3Ce_2Cl_{12}$ and $Ba_3U_2Cl_{12}$ shown in Table 7 is as expected, considering the ionic radii of the M^{3+} cations (*i.e.* $r(Nd^{3+}, VI) < r(Ce^{3+}, VI) < r(U^{3+}, VI)$ [33]), respectively.

3.1.2. Thermodynamic modelling

The thermodynamic model of this system was fitted to the experimental data of Desyatnik et al. [30] and the results of the DSC measurement performed in this work. In the absence of available experimental data, the mixing enthalpy estimated with Davis' method [35], explained in detail in our previous works [14,15], is used as a fitting basis. The phase diagram of the $BaCl_2-UCl_3$ system is shown in Fig. 2, and the mixing enthalpy in Fig. 4. A comparison between the invariant equilibria calculated with the CALPHAD model and the experimental data from Desyatnik et al. [30] is presented in Table 8. The thermodynamic model reproduces the experimental data well, with the exception of the measured invariant equilibria between $x(UCl_3) = 0.5$ and $x(UCl_3) = 0.85$ at $T = 930$ K. These equilibria have not been interpreted by Desyatnik et al. either. Without further information on the nature of these equilibria, we have been unable to incorporate them in the CALPHAD model.

3.1.3. The $SrCl_2-UCl_3$ system

The system $SrCl_2-UCl_3$ has been studied by Desyatnik et al. [30] using DTA. In their discussion of this system, Desyatnik et al. suggest an intermediate compound with the composition $SrUCl_5$ to account for the disappearance of the eutectic event at compositions $x(UCl_3) \leq 0.5$, as well as the appearance of a peritectic event at these compositions.

The CALPHAD model displayed in Fig. 3 was optimized to fit the measured invariant points by Desyatnik et al. as well as the estimated mixing enthalpy shown in Fig. 4. A comparison between the invariant equilibria calculated with the CALPHAD model and the experimental data from Desyatnik et al. [30] is presented in Table 9. Furthermore, the eutectic composition in this system corresponds with the minimum of the mixing enthalpy curve. Based on the analogous system $SrCl_2-NdCl_3$ and $SrCl_2-CeCl_3$, studied in our previous works [14,15], the existence of a solid solution on the $SrCl_2$-rich side of the phase diagram was hypothesized. It is worth pointing out that this solid solution helps accounting for the very flat liquidus line Desyatnik et al. [30] measured in this system at low UCl_3 content. Desyatnik et al. did not include this solid solution in their interpretation of the system. However, due to the lack of DTA experiments below $x(UCl_3) = 0.15$ and the fact that they did not perform crystallographic measurements in this system, it is possible that they did not observe it.

3.1.4. The $BaCl_2-ThCl_4$ system

Gorbunov et al. [36] present an experimental investigation of the system $BaCl_2-ThCl_4$, and found that this system contains two intermediate compounds with compositions Ba_3ThCl_{10} and $Ba_3Th_2Cl_{12}$, respectively. The authors based the existence of these intermediates on the disappearance of the eutectic and peritectic events below certain compositions (*i.e.* $x(ThCl_4) = 0.4$ and $x(ThCl_4) = 0.25$, respectively). No mixing enthalpy data have been reported in the literature, and no mixing enthalpy could be estimated due to a lack of data on similar systems. The phase diagram for this system is presented in Fig. 5, and the calculated mixing enthalpy is given in Fig. 6. A comparison between the invariant equilibria calculated with the CALPHAD model and the experimental data from Gorbunov et al. [36] is presented in Table 10. The CALPHAD model reproduces the available experimental data well, with the exception of the liquidus in the $BaCl_2$-rich region. The lower liquidus in this part of the phase diagram could hint at a high-temperature solid solution of $ThCl_4$ in β-$BaCl_2$, but due to a lack of experimental data this solid solution was not included in the model.

3.1.5. The $SrCl_2-ThCl_4$ system

The thermodynamic assessment of the $SrCl_2-ThCl_4$ system is based on the experimental data by Gorbunov et al. [36] and shows a good agreement with the reported invariant equilibria as shown in Fig. 7. In their work, Gorbunov et al. measured the system using DTA and found it to be a simple binary eutectic. A comparison between the invariant equilibria calculated with the CALPHAD model and the experimental data from Gorbunov et al. [36] is presented in Table 11. No experimental mixing enthalpy data have been reported in the literature, and due to the lack of information from similar systems, no mixing enthalpy could be estimated either. The calculated mixing enthalpy is given in Fig. 6. In is worth noting that due to the low boiling point of $ThCl_4$, the gas phase is also visible on the phase diagram on the $ThCl_4$-rich side in Fig. 7.

The mixing enthalpies of the systems with $ThCl_4$ shown in Fig. 6 show that it is less negative in the $SrCl_2-ThCl_4$ system than in the $BaCl_2-ThCl_4$ system. This is in line with the results observed in our previous work [15], in which we observed similar behaviour for the systems $AECl_2-NdCl_3$. Additionally, the minima of the mixing enthalpy curves are close to the lowest eutectic compositions of each system.

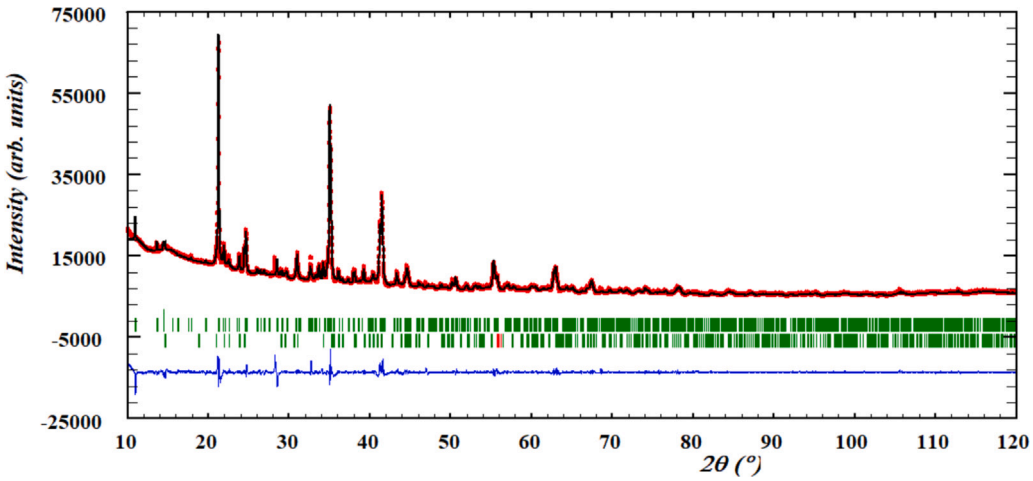

Fig. 1. Profile refinement of the XRD data of the post-DSC sample at x(UCl_3) = 0.2. The phases included in the refinement are α-$BaCl_2$ (SGR *Pnma*, Hull et al. [34]) and $Ba_3U_2Cl_{12}$ (based on $Ba_3Ce_2Cl_{12}$, SGR *I4/m*, Alders et al. [14]). The observed intensity (Yobs, red) is plotted along with the calculated intensity from the refinement (Ycalc, black), and the difference between the two is shown (Yobs-Ycalc, blue). The angles at which reflections occur are shown as well (Bragg positions, vertical lines). Measurement at λ = Cu-Kα.

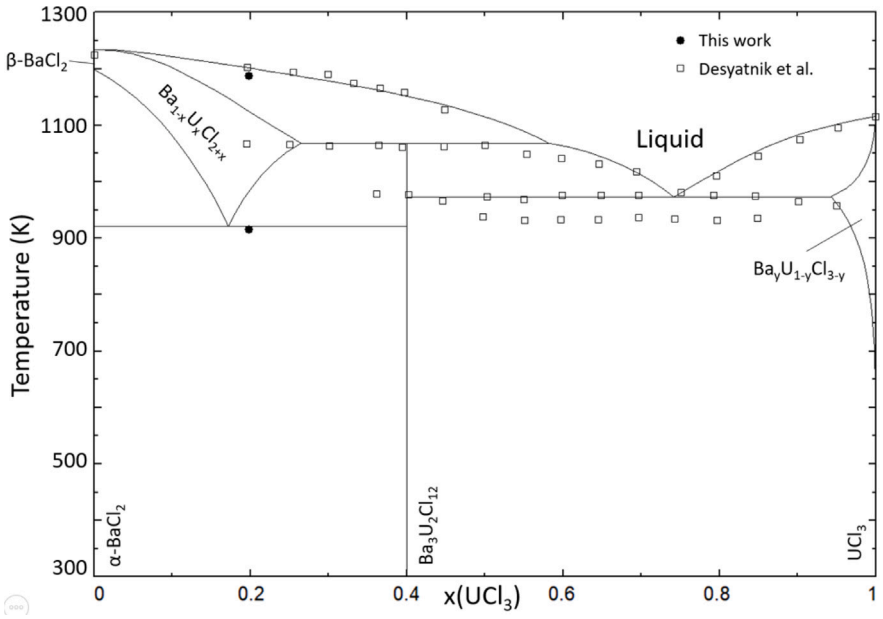

Fig. 2. Phase diagram of the $BaCl_2$−UCl_3 system calculated with the thermodynamic model presented in this work. Experimental data by Desyatnik et al. (open black squares) and this work (closed black circles).

Table 8
Calculated invariant equilibria in the $BaCl_2$−UCl_3 system, as well as experimentally measured values of these invariants from Desyatnik et al. [30]. The number in parentheses is the respective composition of the eutectic from Desyatnik et al.

x(UCl_3)	T (K)		Equilibrium	Invariant reaction
	CALPHAD	Desyatnik et al. [30]		
0	1235	1233	Congruent melting	$BaCl_2$ = L
0.172	921	–	Eutectoid	α-$BaCl_2$ + $Ba_3U_2Cl_{12}$ = $Ba_{1-x}U_xCl_{2+x}$
0.4	1067	1058	Peritectic	$Ba_3U_2Cl_{12}$ = $Ba_{1-x}U_xCl_{2+x}$ + L′
0.742	970	973 (0.750)	Eutectic	$Ba_3U_2Cl_{12}$ + $U_{1-y}Ba_yCl_{3-y}$ = L
1	1113	1106	Congruent melting	UCl_3 = L

3.2. The systems UCl_3−$ThCl_4$ and NaCl−$ThCl_4$−UCl_3

The system UCl_3−$ThCl_4$ has been investigated experimentally by Desyatnik et al. [37] by DTA. Based on the disappearance of the eutectic event below the composition x($ThCl_4$) = 0.25, Desyatnik et al. concluded that an intermediate of composition U_3ThCl_{13} forms in the system. A thermodynamic model was constructed based on the interpretation by Desyatnik et al. and the calculated phase diagram is shown in Fig. 8, showing very good agreement with the experimental data. A comparison between the invariant equilibria calculated with the CALPHAD model and the experimental data from Desyatnik et al. [37] is presented in Table 12. As for the other systems containing $ThCl_4$,

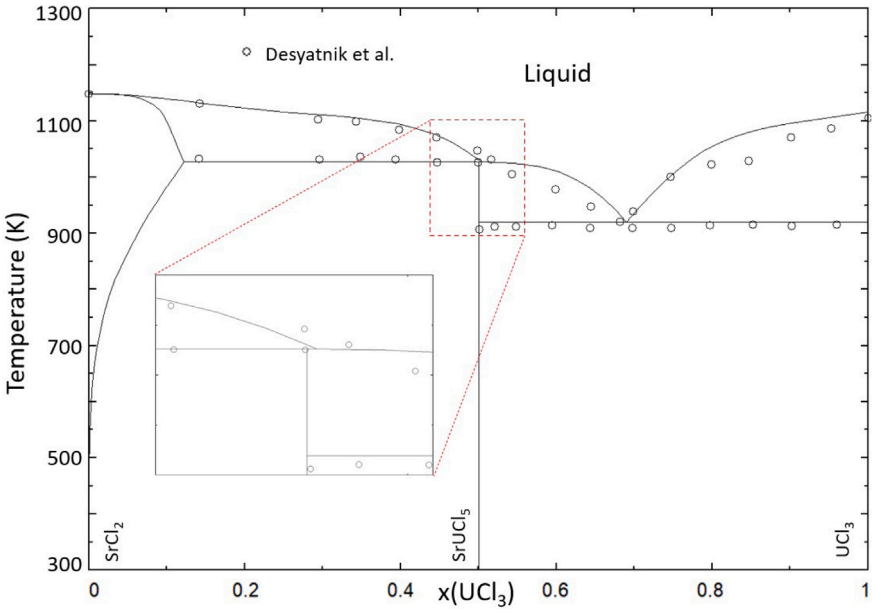

Fig. 3. Phase diagram of the $SrCl_2$−UCl_3 binary system, as calculated with the optimized thermodynamic model. Data from Desyatnik et al. [30] (open black circles).

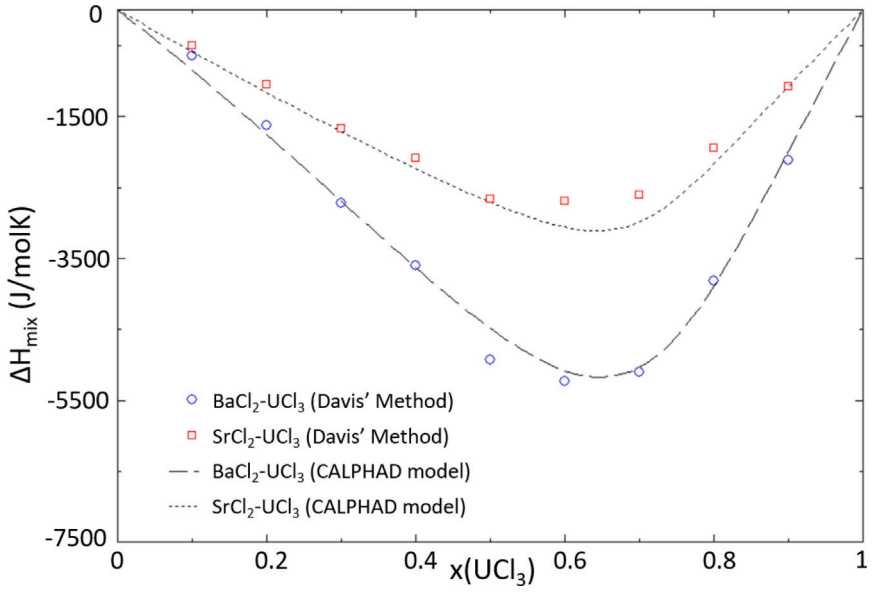

Fig. 4. Mixing enthalpy of the $SrCl_2$−UCl_3 system at T = 1200 K (dotted line) and $BaCl_2$−UCl_3 system calculated at T = 1273 K (dashed line), as calculated with the thermodynamic model. The thermodynamic model well reproduces the data estimated using Davis′ method [35] of $SrCl_2$−UCl_3 (□) and $BaCl_2$−UCl_3 (○).

Table 9
Calculated invariant equilibria in the $SrCl_2$−UCl_3 system, as well as experimentally measured values of these invariants from Desyatnik et al. [30]. The number in parentheses is the respective composition of the eutectic from Desyatnik et al.

x_{NdCl3}	T (K) CALPHAD	Desyatnik et al. [30]	Equilibrium	Invariant reaction
0	1146	1147	Congruent melting	$SrCl_2$ = L
0.5	1125	1115	Peritectic	$SrUCl_5 = Sr_{1-x}U_xCl_{2+x}$ + L′
0.697	915	908 (0.690)	Eutectic	$SrUCl_5$ + UCl_3 = L
1	1113	1106	Congruent melting	UCl_3 = L

the mixing enthalpy data have not been reported in the literature, and no estimation could be made based on similar systems. The mixing enthalpy of this system as calculated with the thermodynamic model is given in Fig. 6.

The thermodynamic models for the systems NaCl−UCl_3 and NaCl−$ThCl_4$ are taken from the respective literature [17,20,38], whereas the models for the interaction of NaCl with the investigated fission products (*i.e.* NaCl-$AECl_2$ (AE = Sr, Ba) and NaCl-$RECl_3$ (RE = Nd,

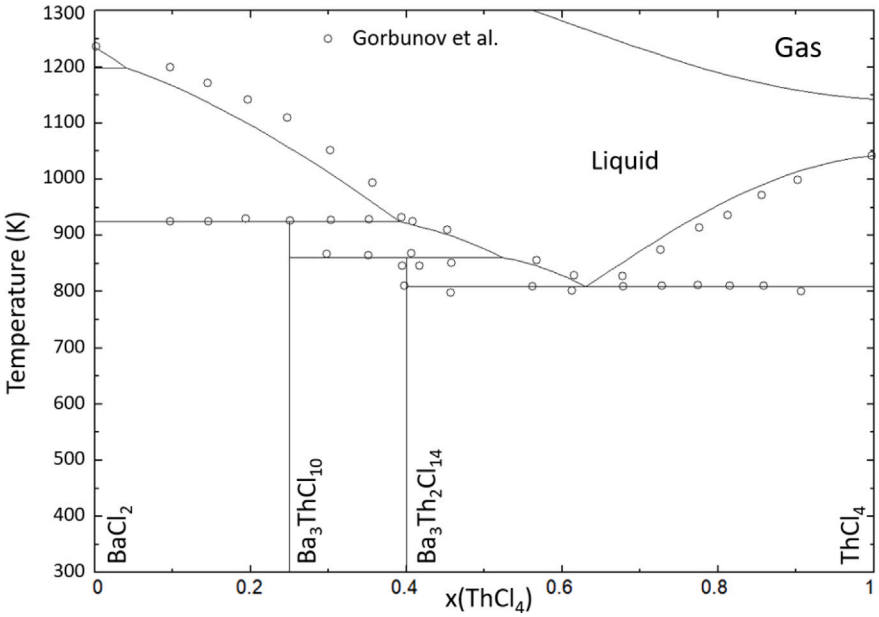

Fig. 5. Phase diagram of the system $BaCl_2$—$ThCl_4$ calculated with the thermodynamic model presented in this work. Experimental data from Gorbunov et al. [36] (open black circles).

Table 10
Calculated invariant equilibria in the $BaCl_2$—$ThCl_4$ system, as well as experimentally measured values of these invariants from Gorbunov et al. [36]. The number in parentheses is the respective composition of the eutectic from Gorbunov et al.

x_{ThCl4}	T (K)		Equilibrium	Invariant reaction
	CALPHAD	Gorbunov et al. [36]		
0	1235	1234	Congruent melting	$BaCl_2$ = L
0.25	924	923	Peritectic	Ba_3ThCl_{10} = α-$BaCl_2$ + L′
0.40	860	858	Peritectic	$Ba_3Th_2Cl_{12}$ = Ba_3ThCl_{10} + L′
0.63	810	808 (0.64)	Eutectic	$ThCl_4$ + $Ba_3Th_2Cl_{12}$ = L
1	1040	1040	Congruent melting	$ThCl_4$ = L

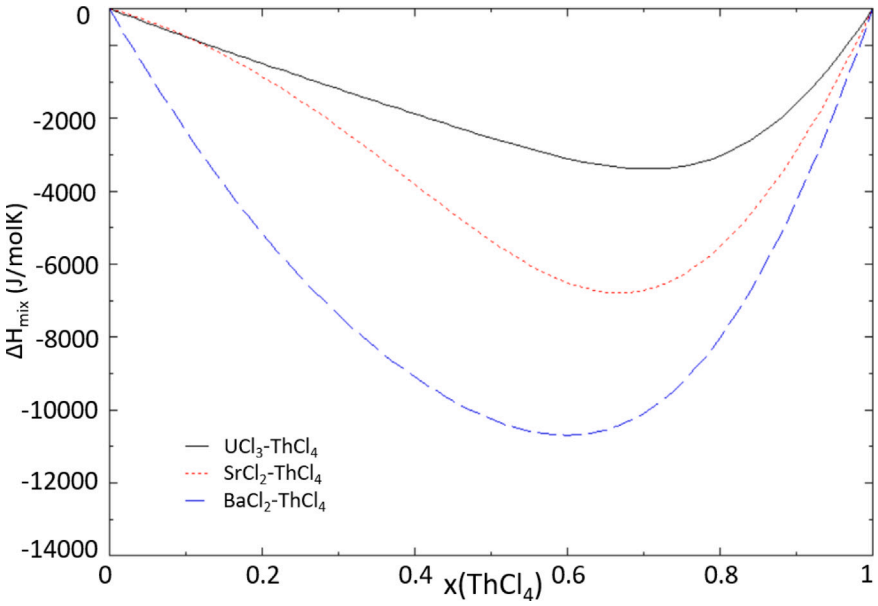

Fig. 6. Mixing enthalpies of the systems $SrCl_2$—$ThCl_4$ (dotted red line), $BaCl_2$—$ThCl_4$ (dashed blue line) and UCl_3—$ThCl_4$ (solid black line) calculated at T = 1200 K with the thermodynamic model presented in this work.

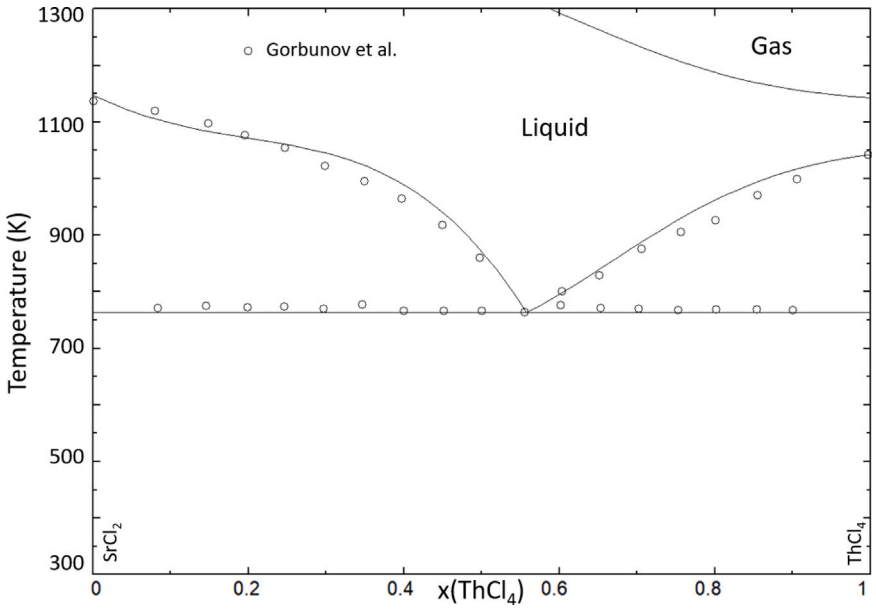

Fig. 7. Phase diagram of the system $SrCl_2$—$ThCl_4$ calculated with the thermodynamic model presented in this work. Experimental data from Gorbunov et al. [36] (open black circles).

Table 11
Calculated invariant equilibria in the $SrCl_2$—$ThCl_4$ system, as well as experimentally measured values of these invariants from Gorbunov et al. [36]. The number in parentheses is the respective composition of the eutectic from Gorbunov et al.

x_{ThCl4}	T (K)		Equilibrium	Invariant reaction
	CALPHAD	Gorbunov et al. [36]		
0	1146	1143	Congruent melting	$SrCl_2$ = L
0.56	761	769 (0.560)	Eutectic	$ThCl_4$ + $SrCl_2$ = L
1	1040	1040	Congruent melting	$ThCl_4$ = L

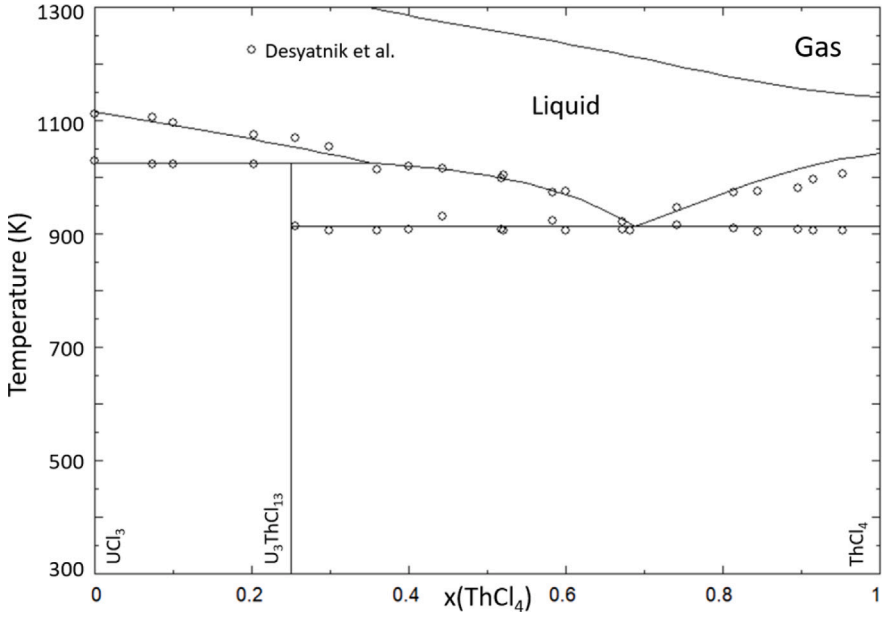

Fig. 8. Phase diagram of the UCl_3—$ThCl_4$ system as calculated with the thermodynamic model presented in this work. Experimental data by Desyatnik et al. [37] (open black circles).

Table 12
Calculated invariant equilibria in the UCl_3−$ThCl_4$ system, as well as experimentally measured values of these invariants from Desyatnik et al. [37]. The number in parentheses is the respective composition of the eutectic from Desyatnik et al.

x_{ThCl4}	T (K)		Equilibrium	Invariant reaction
	CALPHAD	Desyatnik et al. [37]		
0	1113	1110	Congruent melting	UCl_3 = L
0.25	1023	1023	Peritectic	U_3ThCl_{13} = UCl_3 + L′
0.69	912	905 (0.70)	Eutectic	$ThCl_4$ + U_3ThCl_{13} = L
1	1040	1040	Congruent melting	$ThCl_4$ = L

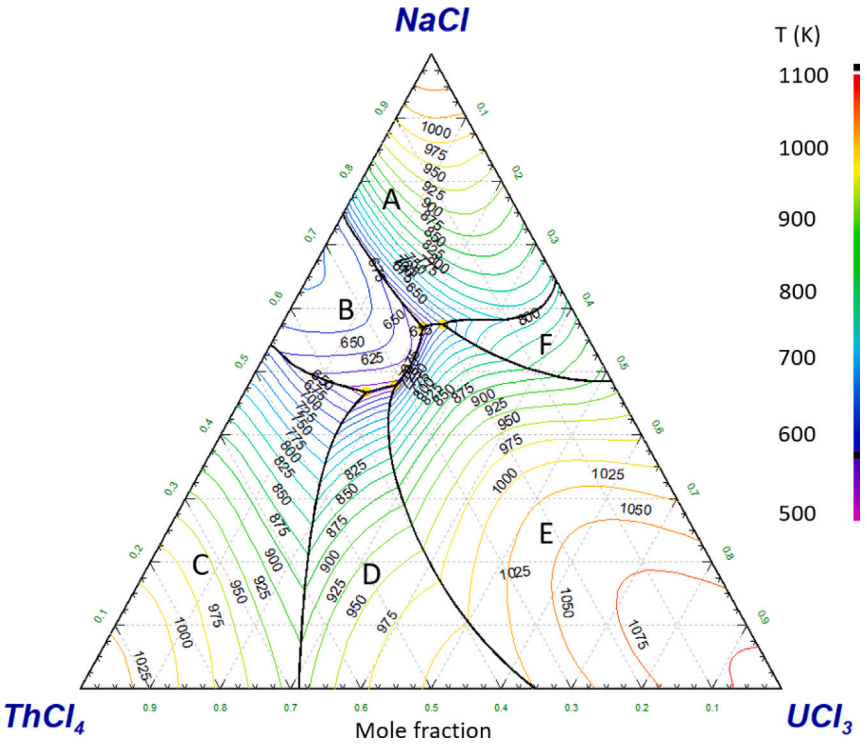

Fig. 9. Liquidus projection of the NaCl−$ThCl_4$−UCl_3 ternary systems. Primary crystallization phases labelled A-F are: NaCl (A), Na_2ThCl_6 (B), $ThCl_4$ (C), U_3ThCl_{13} (D), UCl_3 (E), and NaU_2Cl_7 (F). The calculated invariant equilibria are given in Table 13.

Table 13
Calculated ternary invariant equilibria in the NaCl−$ThCl_4$−UCl_3 system.

x(NaCl)	x($ThCl_4$)	x(UCl_3)	T(K)	Invariant equilibrium
0.575	0.195	0.231	682	NaCl + NaU_2Cl_7 + UCl_3
0.569	0.227	0.204	594	NaCl + Na_2ThCl_6 + UCl_3
0.479	0.310	0.210	593	Na_2ThCl_6 + U_3ThCl_{13} + UCl_3
0.467	0.358	0.175	585	Na_2ThCl_6 + $ThCl_4$ + U_3ThCl_{13}

Ce)) are taken from previous works [14,15,20]. In addition, Dumaire et al. [39] have shown that there is significant ternary interaction in the system NaCl−$ThCl_4$−$PuCl_3$, which we have used in this work to model the NaCl−$ThCl_4$−UCl_3 ternary system. In the same line of reasoning, we have used the work of Dumaire et al. to approximate the ternary behaviour in the systems NaCl−$ThCl_4$−$CeCl_3$ and NaCl−$ThCl_4$−$NdCl_3$.

No experimental data are available in the ternary system NaCl−$ThCl_4$−UCl_3. However, Dumaire et al. [17] showed that significant ternary interaction terms in the NaCl−$ThCl_4$−$PuCl_3$ were necessary in their thermodynamic model. Due to the similar nature of actinides Pu and U, a deviation from ideality is to be expected in the ternary mixture NaCl−$ThCl_4$−UCl_3 as well. For this reason, the ternary excess Gibbs energy parameters presented by Dumaire et al. are used in this work to approximate the ternary interactions in the NaCl−$ThCl_4$−UCl_3 system, as shown in Fig. 9. The calculated ternary invariant equilibria are listed in Table 13.

Table 14
Fuel compositions of interest in this study.

x(NaCl)	x($ThCl_4$)	x(UCl_3)	T_{melt}(K)	Source
0.34		0.66	791	Yingling et al. [38]
0.569	0.227	0.204	594	This work
0.467	0.358	0.175	585	This work (CALPHAD)

4. Application calculations for MSR safety assessment

An example of the potential application of thermodynamic databases in the framework of safety analysis of molten salt react ors is presented here, based on the multi-component database NaCl−$ThCl_4$−UCl_3−$NdCl_3$−$CeCl_3$−$SrCl_2$−$BaCl_2$ presented in this work. These calculations are performed for a NaCl−UCl_3 fuel, containing only a fissile element, and a fuel assembly consisting of NaCl−UCl_3−$ThCl_4$, which also incorporates a fertile element in the fuel matrix.

The fuel compositions of interest in this work are chosen as the composition of the eutectic in the NaCl−UCl_3 binary system, and two ternary eutectic compositions in the NaCl−UCl_3−$ThCl_4$ system. The investigated fuel compositions are presented in Table 14.

With the aim of investigating the effect of the fission products Ba, Sr, Ce and Nd on molten salt fuels, the fission product yields were taken from Taube et al. [40], who performed neutronics calculations for molten chloride fuels in a fast neutron spectrum. While these calculations were performed for a Pu-based fuel and are therefore

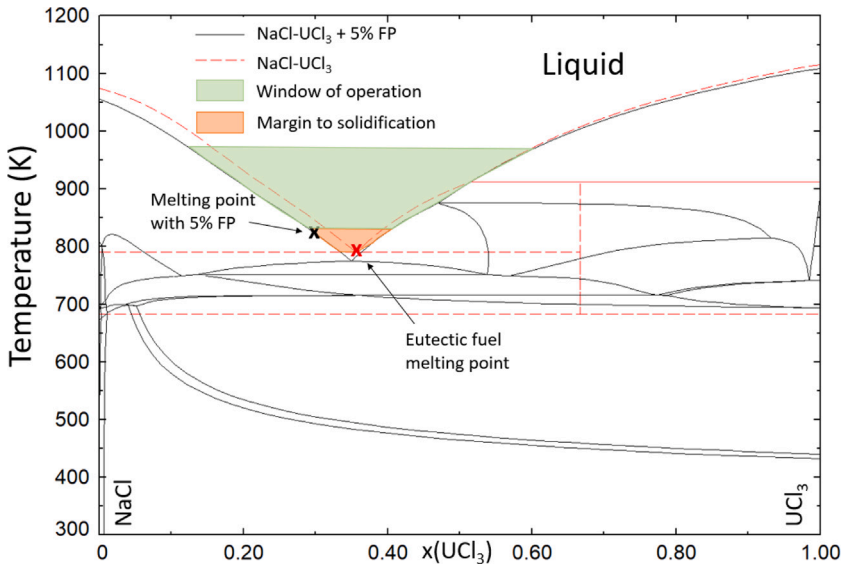

Fig. 10. Phase diagram of the NaCl−UCl_3 system (dashed red line), compared to the same system mixed with 5 mol% fission products Ba, Sr, Ce and Nd (solid black line) using the FP ratios given in Table 15. Indicated on the phase diagram are the melting point of the fresh fuel (black x, {0.65 NaCl + 0.35 UCl_3}) and the melting point of the fuel with 5 mol% fission products (red x, {0.65 NaCl + 0.30 UCl_3 + 0.010 $BaCl_2$ + 0.005 $SrCl_2$ + 0.019 $CeCl_3$ + 0.016 $NdCl_3$}). Additionally, a possible operating window and the margin to solidification are indicated in green and orange respectively.

Table 15
Fission product yields used in the calculations, taken from the work of Taube et al. [40] who performed neutronics calculations for molten $PuCl_3$-fuel in a fast neutron spectrum.

Fission product	Absolute yield (atoms per 100 Pu fissioned)	Relative yield (%)
Ba	9.5	18.7
Sr	5.5	10.8
Ce[a]	19.8	38.8
Nd[b]	16.2	31.7

[a] Also includes the yield of La as fission product.
[b] Also includes the yield of Pr as fission product.

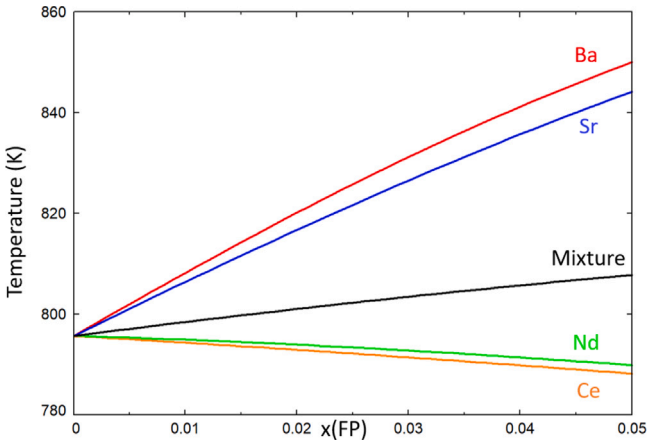

Fig. 11. Calculated change in melting temperature of the {0.65 NaCl + 0.35 UCl_3} fuel mixture (*i.e.* the eutectic composition in the NaCl−UCl_3 system) when replacing up to 5_{mol}% of U by fission products Sr, Ba, Ce and Nd.

not exactly the same in a U-based fuel, they serve as a good first approximation. The approximation is made in our calculations is that all U fissions into Sr, Ba, Ce and Nd. Additionally, because of the similarities in their chemistry and to simplify the experimental and modelling investigations slightly, the yield of lanthanum (La) as fission product was added to the yield of Ce, and the yield of praseodymium (Pr) as fission product was added to that of Nd.

A simple example of how a molten salt system changes upon the addition of fission products is presented in Fig. 10, taking the specific case of the addition of 5 mol% of fission product mixture (Ba, Sr, Ce, Nd, ratio as presented in Table 15). During irradiation, the phase diagram of the fuel with fission products becomes highly complex, shown here by the appearance of many new phase fields and the affected liquidus temperature. These phase fields are calculated to assess whether there is a risk of precipitation of the fissile element. Also shown on this phase diagram are two temperature ranges to consider: (1) up to 50 K above the melting point of the eutectic mixture (i.e. 845 K, red area in Fig. 10), which represents the margin to solidification, and (2) an operating window from 50 to 150 K above the eutectic, which is the operating temperature for a design-based transient (i.e. up to 945 K, green area in Fig. 10). In the example case, it is shown that the melting point upon introduction of fission products stays within the safe temperature range.

The change in the melting temperature of the fuel salt is first analysed for each investigated fission product individually, as well as for a (Ba,Sr,Nd,Ce) mixture. The concentrations used are exaggerated compared to a real scenario for the purpose of visualization of the individual effects. To do this, the change in melting temperature is calculated when the fissile element, in all calculations taken as U, is replaced by an equal amount of fission product up to 5 mol%.

As shown in Figs. 11–13, the fission product that has the largest influence on the melting temperature of the fuel is barium. The reason for this large increase in melting temperature is the formation of the intermediate $Ba_3U_2Cl_{12}$, which precipitates preferentially when Ba is present. The effect of the mixture of fission products (based on Table 15) is also shown in the same figures, where it is clear that the increase in melting temperature is limited and stays within the projected 50 K margin to solidification. The exception here is the last composition in Fig. 13, where the trend is largely governed by the presence of barium, and a large temperature increase is predicted. The primary crystallization phase here is $Ba_3U_2Cl_{12}$, meaning that if the temperature of the reactor becomes too low, there is a risk of precipitation of the fissile material. It must be noted that any possible higher order interactions in the NaCl−$BaCl_2$−$ThCl_4$−UCl_3 system, which have not been modelled in this work, could influence the precipitation calculations shown here.

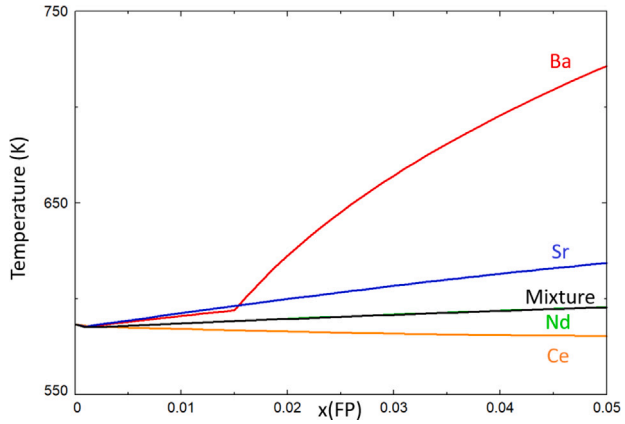

Fig. 12. Calculated change in melting temperature of the {0.467 NaCl + 0.358 $ThCl_4$ + 0.175 UCl_3} fuel mixture (*i.e.* a eutectic composition in the ternary system) when replacing up to 5_{mol}% of U by fission products Sr, Ba, Ce and Nd.

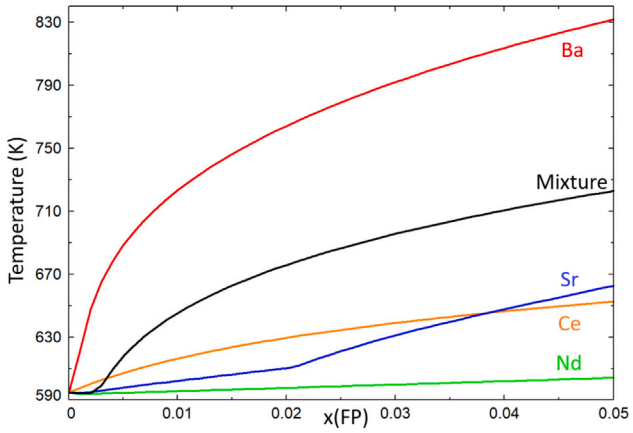

Fig. 13. Calculated change in melting temperature of the {0.569 NaCl + 0.227 $ThCl_4$ + 0.204 UCl_3} fuel mixture (*i.e.* a eutectic composition in the ternary system) when replacing up to 5_{mol}% of U by fission products Sr, Ba, Ce and Nd.

5. Summary and recommendations

In this work, the thermochemical behaviour of $SrCl_2$ and $BaCl_2$ in actinide chloride systems with uranium and thorium has been modelled for the first time. The chemistry of the systems $AECl_2$−UCl_3 (AE = Sr, Ba) is very similar to that of the systems $AECl_2$−$RECl_3$ (RE = Ce, Nd) presented in a previous work [14,15]. In particular, the existence of the solid solution $Ba_{1-x}U_xCl_{2+x}$ and intermediate $Ba_3U_2Cl_{12}$, rather than Ba_2UCl_7 as suggested by Desyatnik et al. [30], were hypothesized based on the simulant $BaCl_2$−$RECl_3$ systems (RE = Ce, Nd), and subsequently confirmed experimentally. The system $SrCl_2$−UCl_3 is characterized by an intermediate compound, $SrUCl_5$, and a solid solution, $Sr_{1-x}U_xCl_{2+x}$, at the $SrCl_2$-rich side of the phase diagram.

The interactions of fission products $SrCl_2$ and $BaCl_2$ (as well as UCl_3) with $ThCl_4$ have moreover been modelled based on experimental data from the literature. The system $SrCl_2$−$ThCl_4$ is a simple binary eutectic system with no apparent solid solubility, while the $BaCl_2$−$ThCl_4$ system is characterized by two intermediate compounds, Ba_3ThCl_{10} and $Ba_3Th_2Cl_{14}$.

With the thermodynamic model presented in this work, the effect of fission products Sr and Ba on the melting behaviour of fuel systems containing UCl_3 or a mixture of $ThCl_4$ and UCl_3 was investigated through application calculations. These calculations showed that, under the conditions imposed in this work, the presence of the fission product Ba in the molten fuel salt could cause precipitation risks due to the formation of the stable $Ba_3U_2Cl_{12}$ intermediate. This hypothesis should be tested in a complementary work that will investigate the chemistry of ternary systems NaCl−$ThCl_4$−MCl_3 (M = U, Ce, Nd) to verify the assumption that their behaviour is similar to that of the NaCl−$ThCl_4$−$PuCl_3$ system, and to explore the interactions in higher order systems.

CRediT authorship contribution statement

Dennis C. Alders: Writing – original draft, Investigation, Formal analysis, Conceptualization. **Max J.A. IJszenga:** Writing – review & editing, Investigation. **Nick T.H. ter Veer:** Writing – review & editing, Resources. **Elisa Capelli:** Writing – review & editing. **Rudy J.M. Konings:** Writing – review & editing, Supervision. **Anna L. Smith:** Writing – review & editing, Supervision.

Declaration of competing interest

The authors declare that they have no known competing financial interests or personal relationships that could have appeared to influence the work reported in this paper.

Acknowledgement

The authors of this paper gratefully acknowledge financial support from the ORANO group.

Data availability

Data will be made available on request.

References

[1] E. Bettis, R. Schroeder, G. Cristy, H. Savage, R. Affel, L. Hemphill, The aircraft reactor experiment—design and construction, Nucl. Sci. Eng. 2 (6) (1957) 804–825.
[2] C. Le Brun, Molten salts and nuclear energy production, J. Nucl. Mater. 360 (1) (2007) 1–5.
[3] S.S. Rudel, H.L. Deubner, B. Scheibe, M. Conrad, F. Kraus, Facile syntheses of pure uranium (III) halides: UF3, UCl3, UBr3, and UI3, Z. Anorg. Allg. Chem. 644 (6) (2018) 323–329.
[4] V. Glushko, L. Gurvich, V. Weitz, et al., Thermodynamic properties of individual substances, vol. 3, (2) Nauka Publishing House, Moscow, 1978, p. 861.
[5] E. Capelli, R.J.M. Konings, Halides of the actinides and fission products relevant for molten salt reactors, Reference Module in Materials Science and Materials Engineering, Elsevier, 2020, pp. 56–283.
[6] H.M. Rietveld, A profile refinement method for nuclear and magnetic structures, J. Appl. Crystallogr. 2 (2) (1969) 65–71.
[7] B. van Laar, H. Schenk, The development of powder profile refinement at the Reactor Centre Netherlands at Petten, Acta Crystallogr. Sect. A: Found. Adv. 74 (2) (2018) 88–92.
[8] J. Rodríguez-Carvajal, Recent advances in magnetic structure determination by neutron powder diffraction, Phys. B 192 (1993) 55–69.
[9] O. Beneš, R.J.M. Konings, S. Wurzer, M. Sierig, A. Dockendorf, A DSC study of the $NaNO_3$−KNO_3 system using an innovative encapsulation technique, Thermochim. Acta 509 (1–2) (2010) 62–66.
[10] G. Höhne, H. Cammenga, W. Eysel, E. Gmelin, W. Hemminger, The temperature calibration of scanning calorimeters, Thermochim. Acta 160 (1) (1990) 1–12.
[11] G. Della Gatta, M.J. Richardson, S.M. Sarge, S. Stølen, Standards, calibration, and guidelines in microcalorimetry. Part 2. Calibration standards for differential scanning calorimetry*(IUPAC Technical Report), Pure Appl. Chem. 78 (7) (2006) 1455–1476.
[12] H. Lukas, S.G. Fries, B. Sundman, Computational thermodynamics: the calphad method, Cambridge University Press, 2007.
[13] Centre for Research in Computational Thermochemistry, FactSage 8.2, feb 2018.
[14] D.C. Alders, J. Vlieland, M. Thijs, R.J.M. Konings, A.L. Smith, Experimental investigation and thermodynamic assessment of the $AECl_2$−$NdCl_3$ (AE=Sr, Ba) systems, J. Mol. Liq. (2024) 123997.

[15] D.C. Alders, D.J. Cette, R.J.M. Konings, A.L. Smith, Experimental investigation and thermodynamic assessment of the $AECl_2$—$NdCl_3$ (AE=Sr, Ba) systems, Phys. Chem. Chem. Phys. (2024) 123997.
[16] D.C. Alders, B.A.S. Rooijakkers, R.J.M. Konings, A.L. Smith, Experimental Investigation and Thermodynamic Modeling Assessment of the NaCl——NaI——$MgCl_2$——MgI_2 Quaternary System, J. Phys. Chem. C (2025).
[17] T. Dumaire, J.A. Ocádiz-Flores, R.J.M. Konings, A.L. Smith, A promising fuel for fast neutron spectrum Molten Salt Reactor: NaCl—$ThCl_4$—$PuCl_3$, Calphad 79 (2022) 102496.
[18] J.A. Ocádiz Flores, R.J.M. Konings, A.L. Smith, Using the quasi-chemical formalism beyond the phase diagram: Density and viscosity models for molten salt fuel systems, J. Nucl. Mater. 561 (2022) 153536.
[19] J.A. Ocádiz Flores, B.A.S. Rooijakkers, R.J.M. Konings, A.L. Smith, Thermodynamic description of the ACl-ThCl4 (a=li, na, k) systems, Thermo 1 (2) (2021).
[20] D.C. Alders, A. Sacristán Civera, M. Wolff, E. Capelli, E.L. Bright, C. Henning, R.J.M. Konings, A.L. Smith, Simulant chemistry for uranium and plutonium molten fuel salts: crystallographic investigation and thermodynamic modelling assessment of the NaCl—$RECl_3$ and NaCl—$MgCl_2$—$RECl_3$ (RE=Ce, Nd) systems, J. Placeholders (2025).
[21] O. Beneš, Thermodynamic database on molten salt reactor systems, 2021.
[22] M. Rand, F.J. Mompean, J. Perrone, M. Illemassène, Chemical thermodynamics of thorium, Chem. Thermodyn. (2008).
[23] N.T.H. ter Veer, W.K. de Vries, C.T.C. Heyning, T.F. Abbink, J.A. Ocádiz Flores, A.E. Gheribi, R.J.M. Konings, A.L. Smith, Insights into the structural dynamics, thermophysical properties, and thermodynamics of the NaCl—$ThCl_4$ and NaCl—UCl_4systems, J. Mol. Liq. (2025) 128590.
[24] G.I.L. van Oudenaren, J.A. Ocadiz-Flores, A.L. Smith, Coupled structural-thermodynamic modelling of the molten salt system NaCl—UCl_3, J. Mol. Liq. 342 (2021) 117470.
[25] I. Barin, G. Platzki, Thermochemical data of pure substances, vol. 304, (334) Wiley Online Library, 1989.
[26] M.W. Chase Jr., NIST-JANAF thermochemical tables, J. Phys. Chem. Ref. Data, Monogr. 9 (1998).
[27] R.J.M. Konings, A. Kovács, Thermodynamic properties of the lanthanide (III) halides, Handb. Phys. Chem. Rare Earths 33 (2003) 147–247.
[28] A.D. Pelton, P. Chartrand, G. Eriksson, The modified quasi-chemical model: Part IV. Two-sublattice quadruplet approximation, Met. Mater. Trans. A 32 (6) (2001) 1409–1416.
[29] P. Chartrand, A.D. Pelton, Thermodynamic evaluation and optimization of the LiCl—NaCl—KCl—RbCl—CsCl—$MgCl_2$—$CaCl_2$—$SrCl_2$—$BaCl_2$ system using the modified quasichemical model, Can. Metall. Q. 40 (1) (2001) 13–32.
[30] V. Desyatnik, B. Dubinin, Y. Melnikov, S. Raspopin, Interaction of uranium(III) chloride with alkaline earth metal chlorides, Russ. J. Inorg. Chem. 20 (1975) 1085–1087.
[31] I. Storonkin, O. Vasilkova, I. Kozhina, Vestnik, Leningr. Univ. 4 (1973) 80–83.
[32] V. Desyatnik, Y. Izmodenov, Y. Melnikov, I. Nichkov, S. Raspopin, Fusibility diagrams of systems based on magnesium and uranium chlorides, Sov. At. Energy 26 (6) (1969) 634–635.
[33] R.D. Shannon, Revised effective ionic radii and systematic studies of interatomic distances in halides and chalcogenides, Acta Crystallogr. Sect. A: Cryst. Phys. Diffr. Theor. Gen. Crystallogr. 32 (5) (1976) 751–767.
[34] S. Hull, S.T. Norberg, I. Ahmed, S.G. Eriksson, C.E. Mohn, High temperature crystal structures and superionic properties of $SrCl_2$, $SrBr_2$, $BaCl_2$ and $BaBr_2$, J. Solid State Chem. 184 (11) (2011) 2925–2935.
[35] H.T. Davis, S.A. Rice, Perturbation theory of the heats of mixing of fused salts, J. Chem. Phys. 41 (1) (1964) 14–24.
[36] L. Gorbunov, V. Desyatnik, S. Raspopin, K. Trifonov, The interaction of thorium tetrachloride with alkaline earth metal chlorides, Russ. J. Inorg. Chem. 19 (1974) 3093–3095.
[37] V.N. Desyatnik, V. Nichkov, Phase diagrams of the systems $ThCl_4$—UCl_3 and $ThCl_4$—$PuCl_3$, Russ. J. Inorg. Chem. 19720, 101–103.
[38] J. Yingling, J. Schorne-Pinto, M. Aziziha, J. Ard, A. Mofrad, M. Christian, C. Dixon, T. Besmann, Thermodynamic measurements and assessments for LiCl—NaCl—KCl—UCl_3 systems, J. Chem. Thermodyn. 179 (2023) 106974.
[39] T. Dumaire, Advances in the chemistry of Molten Salt fuels with emphasis on Fission Products and Corrosion Products (Ph.D. thesis), Delft University of Technology, 2024.
[40] M. Taube, Fast reactors using molten chloride salts as fuel, Technical Report, 1978.